Challenge Journal of CONCRETE RESEARCH LETTERS

Research Article

The effect of tincal-added cement on the attenuation of gamma rays and neutrons

Hayrettin Eroğlu [a,*], İhsan İş [b], Mustafa Engin Kocadağistan [c], Ali Gürol [d]

[a] *Department of Chemical Engineering, Erzurum Technical University, 25050 Erzurum, Türkiye*
[b] *Department of Biomedical Engineering, Erzurum Technical University, 25050 Erzurum, Türkiye*
[c] *Department of Metallurgical and Materials Engineering, Atatürk University, 25240 Erzurum, Türkiye*
[d] *Department of Physics, Atatürk University, 25240 Erzurum, Türkiye*

ABSTRACT

The increasing use of ionizing radiation in nuclear energy, medical diagnostics, radiotherapy, and industrial applications necessitates the development of effective and sustainable radiation shielding materials. In this study, the gamma-ray and fast neutron attenuation properties of cement-based composites incorporating anhydrous tincal obtained from the Balıkesir–Bigadiç region were experimentally investigated. Tincal was dehydrated at 650 °C to remove crystal water and added to Portland cement at ratios of 1%, 5%, and 10% by weight. The research includes gamma and neutron attenuation experiments, compressive strength tests, SEM, and XRD analyses under different parameters. Based on the evaluation of the obtained results, it was concluded that tincal has no effect on gamma attenuation. In contrast, neutron attenuation performance improved significantly with increasing tincal content. However, compressive strength values decreased significantly in tincal-added samples, which presents limitations for structural applications. It is thought that it cannot be used as a load-bearing element in construction, but rather as a cladding material. When considered overall, the effectiveness of the material in terms of neutron attenuation suggests potential applications in the fields of nuclear safety, radiation protection and construction materials. It is predicted that radiation-attenuating composites developed with natural minerals could contribute to the widespread adoption of environmentally friendly material technologies aimed at minimizing toxic waste production.

ARTICLE INFO

Article history:
Received – December 23, 2025
Revision requested – January 22, 2026
Revision received – February 22, 2026
Accepted – March 2, 2026

Keywords:
Cement
Tincal
Boron
Radiation
Neutron attenuation
Gamma attenuation

Citation: Eroğlu H, İş İ, Kocadağistan ME, Gürol A (2026). The effect of tincal-added cement on the attenuation of gamma rays and neutrons. *Challenge Journal of Concrete Research Letters*, 17(2), 135–146.

1. Introduction

Radiation can be defined as the emission of energy from a source in the form of particles or electromagnetic waves that travel in straight lines. Its utilization has been increasing in a variety of fields, ranging from medical applications to industrial operations (Sehhatigdiri 2014). Radiation is generally categorized into two distinct classifications: ionising and non-ionising. It is well established that exposure to ionising radiation, such as alpha and beta particles, X-rays, and gamma rays, poses a significant risk to human health.

The use of X-rays and gamma rays, in particular, for diagnostic and therapeutic purposes in medicine, such as radiation oncology, nuclear medicine, cardiology, and radiology, is quite widespread. Furthermore, nuclear energy is employed as a substantial source of electrical energy generation. Radiation is also utilized in industrial applications across various regions. Furthermore, radiation is utilized in the destruction of microorganisms during the sterilization process. Radiation is employed in the preservation of foodstuffs, the extension of their shelf life, and the eradication of potentially harmful microorganisms. Radioisotopes find application in a variety

* *Corresponding author*. E-mail address: hayrettin.eroglu@erzurum.edu.tr (H. Eroğlu)
ISSN: 2548-0928 / DOI: https://doi.org/10.20528/cjcrl.2026.02.005

of fields, including materials analysis, archaeological research, and the monitoring and control of industrial processes. A variety of legal permits related to radiation are utilized in research settings. Radiation techniques and methods are utilized in research across a wide range of disciplines, including physics, chemistry, biology, archaeology, and materials science. Radiation safety and control are of crucial importance (Karakoç 2024; Yılmaz 2011).

Gamma rays, which are electromagnetic radiation emitted during transitions between nuclear energy levels, have much higher energy and penetration capability than alpha or beta particles. For this reason, high-density materials are generally used for gamma-ray shielding.

As the use of radiation continues to increase, measures to protect against its potentially harmful effects have become imperative. Ionizing radiation has been demonstrated to induce DNA damage, cellular malfunctions, acute effects at high doses, and stochastic effects such as cancer at lower chronic exposures (Eroglu 2009; Görpe 1992). There are three fundamental methods of protection against the harmful effects of radiation: time, distance and shielding.

- Time: In long-term exposures, the exposure dose increases as time increases, resulting in a directly proportional effect. Therefore, the time spent in the environment near the source should be kept as short as possible. Reducing the exposure time is important for direct exposures, but keeping the exposure time short is even more crucial for fluoroscopy due to the high dose (Eroglu 2009; Keskin 2024).
- Distance: The dose exposure increases as one approaches the radiation source. Radiation intensity is inversely proportional to the square of the distance, a phenomenon known as the inverse square law. Appropriate warnings and signs should be installed in areas close to the radiation source (Eroglu 2009; Keskin 2024).
- Shielding: Materials placed between the radiation source and the exposed area, thereby reducing its intensity, are referred to as shielding materials. Protection is achieved by creating a barrier with materials that prevent the passage of the radiation source. Shielding should be made with materials and thickness appropriate to the type, energy, and intensity of each radiation. Lead shielding should be used to protect against ionizing radiation. Special lead-lined extraction rooms, lead barriers, and leaded personal protective equipment can effectively block ionizing radiation (Eroglu 2009; Keskin 2024). In addition, Yılmaz (2011) investigated the gamma attenuation potential of tincal-based concrete, an alternative to lead shielding.

Concrete is one of the most widely used construction materials owing to its engineering performance, cost efficiency, and durability. Nevertheless, cement-based materials are increasingly being reconsidered from a sustainability perspective because Portland cement production is associated with considerable environmental impacts. Accordingly, mineral additives, industrial by-products, nano-additions, and alternative binder systems have attracted growing attention for improving the mechanical, durability-related, and functional performance of cement-based composites (Abutaha and Çelik 2025; Tarhan and Tarhan 2025; Srivastava et al. 2025). These materials can be tailored through binder composition, particle grading, and admixture selection; however, their effectiveness strongly depends on chemical compatibility, replacement level, particle packing, and their influence on hydration-related products (Al-Safi et al. 2025; Turan et al. 2025; Shaheen et al. 2025). Therefore, when natural mineral additives are incorporated into cementitious systems for specific functional purposes, such as radiation shielding, their contribution must be evaluated together with their possible effects on mechanical integrity and material performance.

Tincal, also known as borax, a boron mineral, appears colorless and transparent in its pure form. However, in areas where it is layered with clay and in fine-grained form, it can turn pale pink, yellowish-orange, and gray under the influence of external substances (Durak 2011). A review of scientific literature suggests that boron oxide may have radiation shielding properties. Studies have shown that:

In a previous study, Erdoğan (1998) produced different types of cement by adding ground boron minerals to cement and examined their physical and mechanical properties. In addition, an evaluation was conducted of the shielding potential of boron minerals when employed in concrete, utilizing theoretical approaches. In light of the findings, it was concluded that boron mineral addition exerted a favorable influence on shielding performance (Erdoğan 1998).

Kharita et al. (2008) investigated the attenuation coefficients of concrete produced from aggregates commonly used in Syria for gamma rays (^{137}Cs and ^{60}Co isotopes) and neutrons (Am-Be source). The concretes were produced by mixing black beach sand, hematite, dolomite, and serpentine with beach sand in varying proportions. The results showed that concretes containing hematite were more effective in providing protection against both types of radiation.

Experiments were conducted by Henrie (1962) on concrete samples containing boron oxide, colemanite, and boron, and the radiation shielding capacity of the concrete's chemical components was analyzed. The study demonstrated that boron-added heavyweight concretes offered advantages not only in terms of effective shielding performance but also in terms of cost.

In a study conducted by Sychev (1967), the shielding potential of concrete samples prepared using hematite minerals against neutrons emitted from a beryllium source were investigated. In this context, evaluations were made considering five different neutron energy levels ranging from 170 MeV to 660 MeV (Sychev 1967).

Erdoğmuş et al. (2011) investigated the effects of adding different mixtures of colemanite concentrator waste and Karabük slag to Portland cement on the mechanical properties of the cement. Additionally, the effect of adding different ratios of Na_2CO_3 to Portland cement on the mechanical properties of the cement were investigated. The colemanite concentrator waste, slag, gypsum, and clinker used in the experiments were chemically analyzed using XRF. The mechanical properties examined in the study included compressive strength, setting time, volumetric expansion, and normal consistency water.

The findings were compared with Turkish Standards (TS), and the research concluded that colemanite concentrator waste and Karabük slag can be utilized appropriately in cement production.

Uğurlu et al. (2004) investigated the usability of solid waste, called "clay paste," generated during the concentration of borax mineral during tincal production, in cement. For the cement study, ground clay paste waste was added to Portland cement mortar at different ratios, and fresh and hardened concrete tests were conducted on the resulting mortar samples. These tests investigated the behavior of clay paste in cement and its effect on cement mortar samples. The results were compared with reference samples and Turkish Standards (TS). The results indicate that borax-containing clay paste waste can be used as a retarder in mortar or concrete, and that low percentages of clay paste waste can increase the impermeability of concrete.

Akkurt et al. (2010) conducted a study using heavyweight concretes produced using barite and lead. They measured linear attenuation coefficients using radioactive sources with energies of 0.662 MeV, 1.173 MeV, and 1.332 MeV using a NaI(Tl) detector. The results were compared with XCOM data. The results revealed that barite and barite-added heavyweight concretes are good gamma-ray absorbers, but their shielding properties are lower than those of lead.

Korkut et al. (2012) carried out a theoretical and experimental investigation in order to ascertain the neutron attenuation properties of colemanite, ulexite and tincal. The researchers discovered that the attenuation of neutrons in these materials is predominantly determined by the density of boron atoms within them. This is due to the fact that boron, particularly the ^{10}B isotope, exhibits a high thermal neutron capture cross-section. The total macroscopic neutron cross sections, denoted by Σ, exhibited a systematic increase with increasing boron content, thereby confirming the predominant role of boron in neutron attenuation.

A study published by Yang et al. (2024) investigated the neutron shielding performance of various boron-containing particles within aluminum-based composites for proton therapy and boron neutron capture therapy (BNCT) applications using Monte Carlo simulations, and showed that increasing boron content significantly improved neutron attenuation efficiency.

Furthermore, Kim et al. (2025) found that high-density boron nitride nanotube (BNNT) composites provide effective shielding against solar-space radiation; this study demonstrates that BNNTs represent a step forward in both mechanical and neutron shielding performance.

In addition, another study by Kiani et al. (2025) addresses the design of multifunctional polymer-nanocomposites and reveals that nanodispersion of boron carbide improves neutron shielding properties.

When boron ore is used in an anhydrous form, the boron compound directly participates in chemical reactions, resulting in lower energy consumption and improved process efficiency. Anhydrous boron exhibits higher chemical activity, enabling more controlled reactions, reduced processing time, and lower overall costs. In contrast, hydrated boron minerals may release crystal water abruptly during heating, leading to foaming, cracking, and volume expansion, which can cause defects in products, particularly in glass, ceramic, and metallurgical applications. The anhydrous form significantly minimizes these risks. From a logistical perspective, crystal water represents unnecessary mass and increases transportation and storage costs. Anhydrous boron ores are lighter, more stable, and less sensitive to moisture. Moreover, industrial processes require water to be introduced separately and in a controlled manner; the uncontrolled presence of crystal water can negatively affect reaction balance, viscosity, and melting behavior. Use of Anhydrous Boron in Cement; in cement systems, boron compounds act as strong setting retarders. When hydrated boron is used, the sudden release of crystal water disrupts cement hydration, causing excessive and unpredictable setting delay. The use of anhydrous boron provides a more predictable and controllable setting behavior. Cement hydration primarily involves the reaction of C_3S and C_2S phases with water. Hydrated boron minerals introduce irregular water into the system, delay C–S–H gel formation, and reduce early-age strength. Anhydrous boron enables precise control of the water-to-cement ratio, leading to a more homogeneous microstructure and improved compressive strength. In addition, anhydrous boron is more compatible with standards such as TS EN and ASTM, facilitating quality control (Jiri et al. 2014; Davraz 2010; Özdemir and Öztürk 2003; Olgun et al. 2007; Filazi et al. 2022).

The present study is concerned with the preparation of tincal-added cement samples, the determination of their physical and mechanical properties, and the experimental investigation of their X- and gamma-ray and neutron attenuation capacity.

2. Materials and Methods

2.1. Materials

In this study, tincal ($Na_2B_4O_7{\cdot}10H_2O$), a primary boron mineral, was used to investigate its neutron beam attenuation properties. The cement used in the experiments was Portland cement (CEM I 42.5 R) supplied by the Aşkale Cement Factory. No additional analysis was performed, as commercially available cement with a known composition was used.

Tincal, a natural borate mineral with a high boron content, was obtained from the Balıkesir-Bigadiç/Türkiye region. Before being used in experimental studies, it underwent preliminary preparation processes such as grinding, drying, and sieve analysis. The tincal ore to be used in the heat treatment experiments was first reduced to 500 grams by taking 1 kg samples from 2 kg of run-of-mine ore using appropriate sampling methods as preparation for particle size reduction. Crushing was performed in a jaw crusher to reduce the particle size to 250 microns (60 mesh), and grinding was performed in a ball mill to obtain a particle size of 45 microns (325 mesh). After obtaining samples with the desired particle size, they were subjected to sieving in 200 g portions. The tincal ore samples were sieved using a mechanical sieve, and the resulting samples were prepared for heat

treatment experiments. The reason for using a particle size of 45 microns is to ensure a similar size to the cement used and to obtain a more homogeneous composition during mixing. Following these processes, the samples were reduced to a particle size of 45 μm and finally heat-treated at 650 °C to remove the crystal water, resulting in anhydrous sodium tetraborate.

The chemical analysis of the ore was determined at Atatürk University DAYTAM using the XPS method. Using the data obtained from the XPS results, the amounts of B_2O_3, H_2O, Na_2O, and CaO in the ore composition were compared and verified with the stoichiometrically calculated amounts and the analysis results of the ore source (Table 1). According to XPS and chemical analysis results of tincal ore, it was determined that tincal contains 47.12% H_2O. As a result of weight difference calculations, H_2O content was reduced to 1% after heat treatment and used in experiments.

Table 1. XPS analysis results of tincal ore.

Compound	Tincal (%)
B_2O_3	36.65
Na_2O	16.23
H_2O	47.12

2.2. Methods

2.2.1. Production of concrete

The concretes examined in this study were produced at the Civil Engineering Department Laboratory of Erzurum Technical University. Three types of concrete were produced in this study: standard concrete and tincal-added concrete. First, cement-only samples were prepared for comparison. Then, 1%, 5%, and 10% tincal were added to each cement sample, sequentially and separately. The water/binder ratio was set at 0.20 in the experiments. The temperature of the sample was measured with a digital thermometer, and the mixing water temperature was determined to be between 25-30 °C. The prepared samples were placed in 5x5x5cm cube sample molds. The samples were kept in their molds for 24 hours and then removed from the molds. During the curing process, the samples were maintained in a constant temperature environment (24 °C), and the ambient temperature and relative humidity were regularly monitored with a digital thermometer. The standard used for determining the setting time is TS EN 196-3 (2016), and the experiments were carried out according to this standard.

2.2.2. Unconfined pressure test

The compressive strength of the concrete produced within the scope of this study was measured at the Department of Civil Engineering, Erzurum Technical University (Fig. 1). Experimental studies were carried out in accordance with the TS EN 12390-3 (2010) standard, and compression was applied to the samples with a constant loading rate until the maximum load capacity was reached (TS EN 12390-3 (2010), is an official standard that specifies the methods of compressive testing performed to measure the strength of concrete). The test sample was placed between the loading head of the testing machine and the test head, and care was taken to ensure that the samples were placed perpendicular to the direction of concrete pouring. The samples were placed centrally on the lower loading head of the machine. The highest load read from the indicator was recorded, and the compressive strength was calculated using the following formula (Uzbaş 2019).

$$\sigma = \frac{P}{A} \tag{1}$$

Here, compressive strength (σ) is the ratio of the maximum load (P) the sample carries at the moment of fracture to the cross-sectional area (A) subjected to compression.

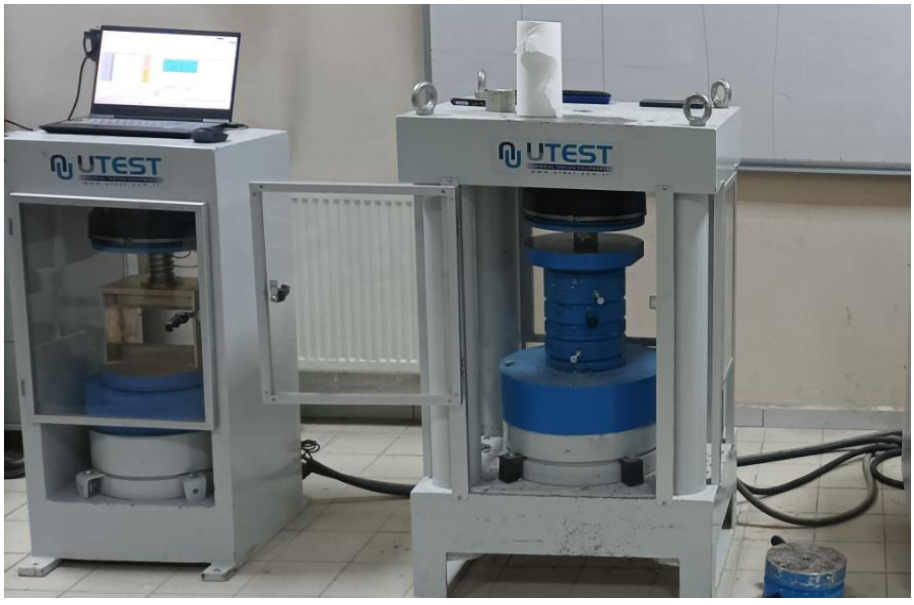

Fig. 1. Unconfined pressure testing apparatus.

2.2.3. Gamma measurements

The experimental measurements undertaken in relation to the attenuation coefficient of the concrete produced as part of the study were conducted at the High Energy Spectroscopy Laboratory, which is housed within the Physics Department at Atatürk University's Faculty of Science. The experimental setup utilized in the study is illustrated in Fig. 2. In the experiment, the VEX (variable energy source) and Ba-133 radioisotope were utilized as the source. In the experiments utilising VEX, the distances between the source and the sample, and between the sample and the detector, were 4.0 cm and 6.0 cm, respectively. The live time in all measurements was set to 1800 s in order to obtain sufficient counting statistics. The Rb, Mo, Ag and Tb K X-rays, as well as the 59.54 gamma rays, are emitted from Am-241 radioisotopes and subsequently scattered elastically from a Cu foil on a VEX source were used in the calculations. The Ba-133 source has a specific activity of approximately 2.73 mCi, emitting gamma rays with energies of 53.155 keV, 81 keV, 276.39 keV, 302.85 keV, 356.01 keV, and 385.851 keV. The distances between the source and the sample, and between the sample and the detector, were 10 cm and 6 cm, respectively.

The intensity of a photon flux, I_0, decreases with increasing thickness, t, of an absorbing material. The decrease in intensity is described by the Lambert-Beer law (Yılmaz 2011) as the linear attenuation coefficient (LAC), given by the following equation:

$$\mu = -\frac{1}{t}\ln\left(\frac{I}{I_0}\right) \quad (\text{cm}^{-1}) \tag{2}$$

However, the mass attenuation coefficient (μ/ρ), defined as the ratio of the linear attenuation coefficient (μ) to the sample density (ρ) and does not change depending on the phase of the material, is more commonly used. The mass attenuation coefficients (MACs) are determined using the intensity values measured experimentally in the experimental geometry shown in Fig. 2 from the equation:

$$\left(\frac{\mu}{\rho}\right) = -\frac{1}{\rho t}\ln\left(\frac{I}{I_0}\right) \tag{3}$$

where ρt is called the mass thickness (g/cm^2). The unit of the mass attenuation coefficients is cm^2/g.

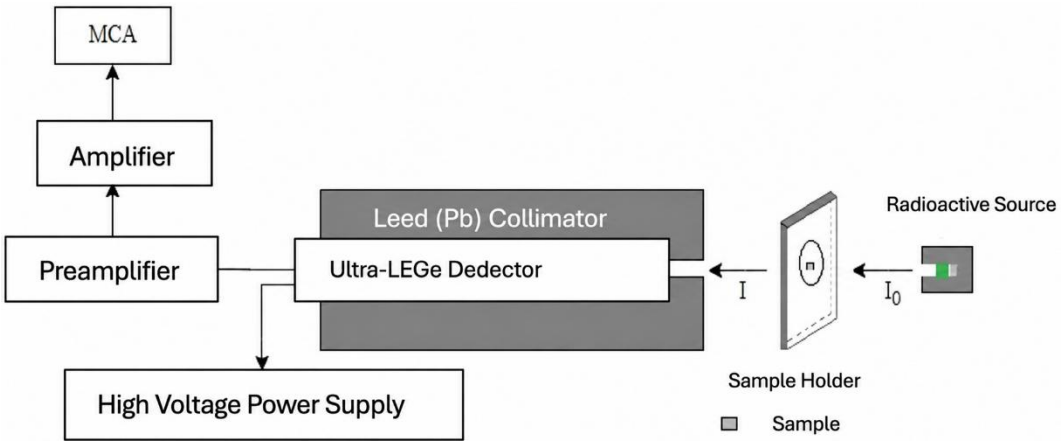

Fig. 2. Experimental setup for gamma ray attenuation.

2.2.4. Neutron attenuation experiments

The experimental measurements undertaken in relation to the attenuation coefficient of the concrete produced as part of the study were conducted at the High Energy Spectroscopy Laboratory, which is housed within the Physics Department, Faculty of Science, Atatürk University.

The measurement of the neutron absorbed dose rate was conducted using a ^{241}Am/Be fast neutron source, which emits 2–11 MeV neutrons. The Canberra NP100B-BF_3 gaseous neutron detector and the Canberra ADM606 series of digital rate meters (RADACs) were utilized in the experiments. The experimental set-up for neutron dose rate measurements is illustrated in Fig. 3. A comprehensive explanation of the properties of the neutron source, detector, and experimental set-up is provided by Korkut et al. (2012).

Neutron experiments are evaluated experimentally by using

$$\Sigma_t = -\frac{1}{Bt}\ln\left(\frac{I}{I_0}\right) \tag{4}$$

where t is thickness of the sample (cm), B is the buildup factor (equal to 5 for Am-Be fast neutron source) Σ_t is the macroscopic removal cross-section which is a measure of the neutron shielding ability for the mean energy of neutron flux having incident dose rate I_0 (μSv/h) and I is dose rate of the transmitted neutron flux (μSv/h) (Wang et al. 2015).

The effective removal cross-section, $\sum R$ (cm^2/g), is a measure of the probability of a fast or fission energy neutron's first collision with the shielding material it faces (Singh and Badiger 2014). The value of $\sum R$ can be calculated by dividing $\sum_t$ by density ρ for an element and evaluated by the mixture rule for a compound or mixture, theoretically. Besides, the effective removal cross-section, $\sum R$ (cm^2/g) is experimentally given by

$$\Sigma R = \frac{\Sigma_t}{\rho} = -\frac{1}{B\rho t}\ln\left(\frac{I}{I_0}\right) \tag{5}$$

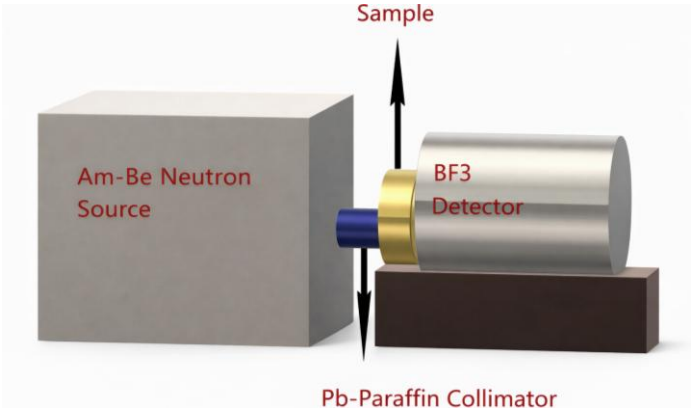

Fig. 3. Experimental setup for neutron attenuation experiments.

2.2.5. X-ray diffraction (XRD)

XRD analysis of the concretes produced within the scope of this study was measured using a GNR-Explorer device at High Technology Application and Research Center (YUTAM), Erzurum Technical University.

Calculating compound or phase compositions from oxide components can be accomplished using both theoretical and experimental methods. X-ray diffraction (XRD) has been successfully used for many years to determine mineral concentrations. Since 1958, various studies have been conducted on the use of XRD analysis in determining cement compositions (Winter 2012).

Concrete, a composite material, exhibits complex behavior due to its high cement content. Microstructural differences from the cement paste have been observed, particularly at the cement-aggregate interface. The formation of new compounds as a result of exposure to various aggressive environmental conditions and the formation of characteristic structures during the natural deterioration processes of concrete have made X-ray diffraction (XRD) analysis an important and essential method for investigating service life, durability, and related product performance (Ramachandran et al. 2000).

2.2.6. Scanning electron microscope (SEM)

SEM/EDX (Scanning Electron Microscopy with Energy Dispersive X-ray Spectroscopy) analyses were performed using FEI QUANTA FEG 250 devices at Erzurum Technical University, High Technology Application and Research Center (YUTAM). SEM images were acquired under the following conditions: kV: 15, Magnification: 10000, Takeoff: 30.1, Amp. Time (µs): 7.68, Resolution: (eV)125. SEM, thanks to its equipment that allows X-ray microanalysis and digital image analysis, enables three basic processes to be carried out on a sample. These processes are; examination of the microstructure of the sample through SEM images, determination of chemical components through X-ray microanalysis, and dimensional measurements through digital image analysis (Winter 2012).

A dosage analysis was performed using SEM and XRD because, according to the analysis results, XRD analysis was performed on the sample that yielded the most suitable result. It is known that the microstructure results cannot be generalized to other dosages.

2.2.7. Heat treatment

The use of boron in the cement sector has become widespread, but boron ores are suitable for use up to a maximum of 2% water content (Kocadağistan and Arslan 2024). Tincal was dewatered in a muffle furnace at 650 °C for 6 hours. Following the heat treatment, the chemically bound water removal rate was calculated by taking the weight differences of tincal ores. According to the calculations, 98% water removal was achieved in both ores (Ataç 2024).

3. Research Findings and Discussion

Cement and tincal mixtures with 1%, 5%, and 10% dehydrated tincal were investigated, and their gamma and neutron attenuation values are given below. Analysis of these values revealed that the best values were obtained with 5% tincal, and SEM and XRD analyses were performed based on these values (Fig. 4). Furthermore, unconfined compression tests of the samples giving the best attenuation values were examined, and their suitability as building materials was evaluated.

3.1. Gamma attenuation tests of tincal additive cement

The Gamma ray attenuation results of the samples of the mixtures are given in Table 2.

Table 2 presents the mass attenuation coefficients μ/ρ at different incident photon energy (E, keV) for samples with different tincal doping ratios (1%, 5%, and 10%). When the data are evaluated in the context of the material's interaction with electromagnetic radiation, it is observed that the linear attenuation coefficient systematically decreases with increasing dopant content. This suggests that the photon attenuation capacity of the material decreases with increasing tincal doping.

The PyMCA software (Sole et al. 2007) was utilized for the determination of I and I_0. The peaks were modelled as being fitted to a Gaussian function with an exponential background. It was determined that the minimum counts of both I and I_0 exceeded 10^4. In order to obtain the background under all peak regions, an exponential polynomial background was utilised, and the software simultaneously calculated both the Gaussian and background at the peak region.

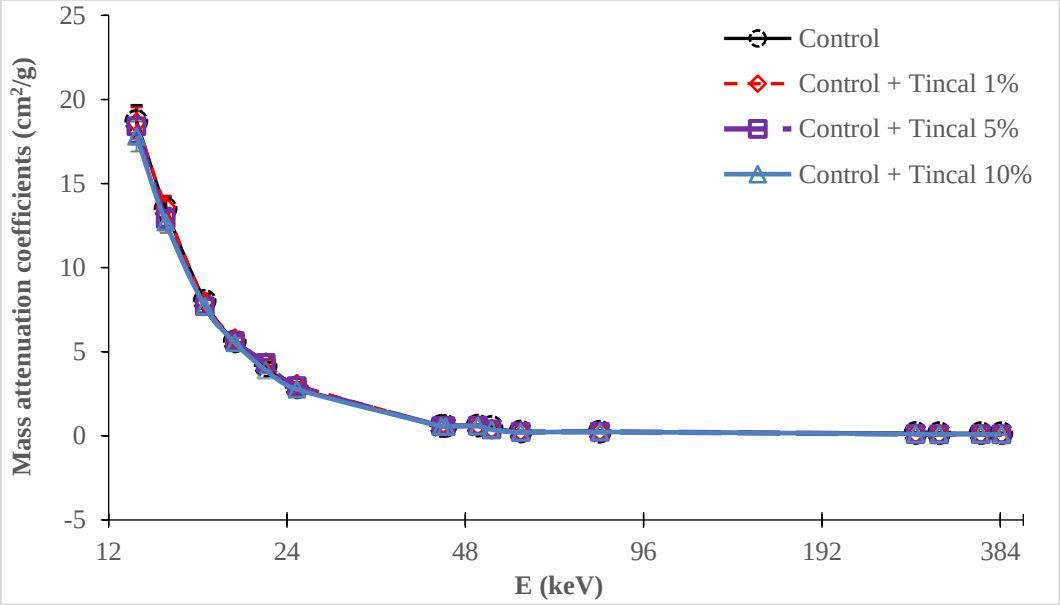

Fig. 4. Mass attenuation coefficients changes of cement samples including tincal with incident X or gamma rays.

Table 2. Measured mass attenuation coefficients μ/ρ (cm²/g) of samples.

E (keV)	Control	Control + 1% Tincal	Control + 5% Tincal	Control + 10% Tincal
13.375	18.7	18.6	18.4	17.8
14.980	13.5	13.6	12.9	12.7
17.443	8.02	7.95	7.71	7.70
19.607	5.60	5.77	5.63	5.53
22.103	4.16	4.34	4.33	3.91
24.942	2.87	3.05	2.95	2.77
43.737	0.580	0.589	0.570	0.568
44.470	0.575	0.583	0.573	0.562
50.391	0.596	0.605	0.598	0.586
53.155	0.521	0.400	0.379	0.375
59.537	0.243	0.260	0.232	0.222
81.000	0.236	0.256	0.240	0.233
276.390	0.160	0.113	0.107	0.107
302.850	0.154	0.091	0.089	0.090
356.010	0.153	0.091	0.090	0.090
385.851	0.148	0.085	0.087	0.086

In our experiments, the standard deviations of peak areas were approximately 1%. The thickness of the samples, which were shaped as rectangular prisms, was measured using a Vernier. The mass of each sample was measured using a high-precision scale. Finally, the thickness uncertainties were found to be less than 1%.

A quantitative analysis was conducted on the density of each sample. This involved calculating the measured mass and volume of the samples, using their known dimensions. It was evident that each measurement reflected its associated uncertainty with respect to the density value. The maximum uncertainties in mass thickness (ρt) employed in the calculations were approximately 2%. It is important to note that the final uncertainties are such that the mass attenuation coefficients listed in Table 2 are less than 3%.

The μ/ρ values demonstrate different behaviors for different energies. In order to proceed, it is necessary to engage in a discussion regarding the alterations in μ/ρ values across three distinct energy domains.

- Low Energy Range (13.375 – 25.942 keV): Tincal dopant has been demonstrated to exhibit a more significant effect on the mass attenuation coefficient μ/ρ. For instance, at 13.375 keV, the undoped control sample displays a value of 18.7, whereas this value diminishes to 17.8 in the 10% tincal-doped sample. This finding

suggests that the tincal doping may impede the interaction of low-energy photons within the material.

- Mid-Energy Range (43.737–81 keV): The tincal dopant effect remains consistent, yet the disparities are more constrained. Within this range, an increase in the doping rate results in a slight decrease in the mass attenuation coefficient μ/ρ.
- High Energy Range (276.39 – 385.851 keV): The tincal dopant effect has reached a minimal level, and the difference between the measured mass attenuation coefficients μ/ρ has decreased considerably.

A general assessment reveals that tincal additions alter the photon absorption properties of cement-based composite materials, and that this change varies with photon energy. It appears that increasing tincal content leads to a decrease in the material's photon absorption capacity, particularly for low-energy photons. These findings provide important insights into the potential role of tincal additions in radiation permeability and structural shielding applications.

3.2. Neutron experiments

The results of the neutron attenuation experiments are given in Table 3 and Fig. 5. The detector measures the dose rate for 100 seconds (one measurement per second and 100 measurement). We repeat the measurements ten times for each sample. We then calculate the mean values of I and I_0 and their standard deviations, which are used as uncertainties. These uncertainties are less than 1% for each sample. The uncertainties at the macroscopic and effective removal cross sections are 2% and 3%, respectively.

The data in Table 3 demonstrate the effects of tincal addition on the neutron attenuation behavior of cement-based samples. As tincal addition increases, a decrease in transmitted light intensity is observed, indicating that the material becomes more effective attenuator against neutrons. Particularly with 5% and 10% tincal additions, the macroscopic and effective removal cross sections increase significantly. This phenomenon is the result of interactions between neutrons and boron nuclei, particularly those of the ^{10}B isotopes. Consequently, in addition to cement, tincal has the potential to enhance the attenuation performance of cement-based composites against neutron radiation.

3.3. XRD analysis evaluation (5% tincal added sample)

The X-ray diffraction (XRD) pattern of a tincal-added cement sample allows the determination of its crystal structure and mineralogical composition. The graph presents intensity values corresponding to the 2θ angle, and these data are used to identify the crystalline phases within the sample (Fig. 6).

Table 3. Tincal neutron attenuation experiment results.

Sample	t (cm)	ρ (g/cm³)	Σ_t (cm^{-1})	ΣR (cm^2/g)
Control	0.540	1.8245	0.248	0.136
Control + Tincal 1%	0.540	1.8087	0.313	0.173
Control + Tincal 5%	0.540	2.1424	0.381	0.178
Control + Tincal 10%	0.540	1.8476	0.373	0.202

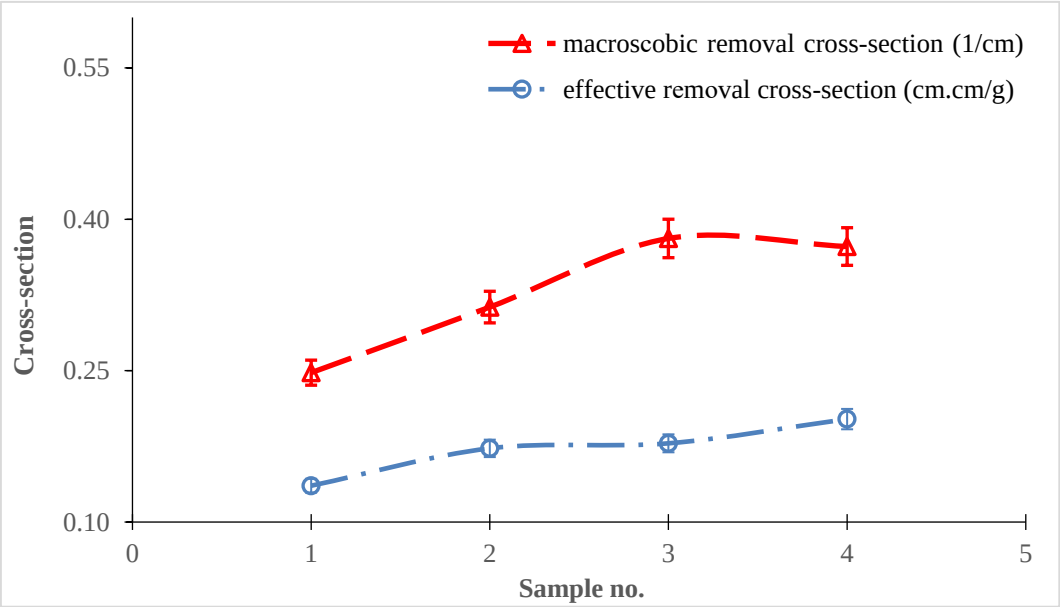

Fig. 5. Neutron experiment results. On the horizontal axis, 1 represents plain cement, and 2, 3, and 4 represent cement with 1%, 5%, and 10% tincal additive, respectively.

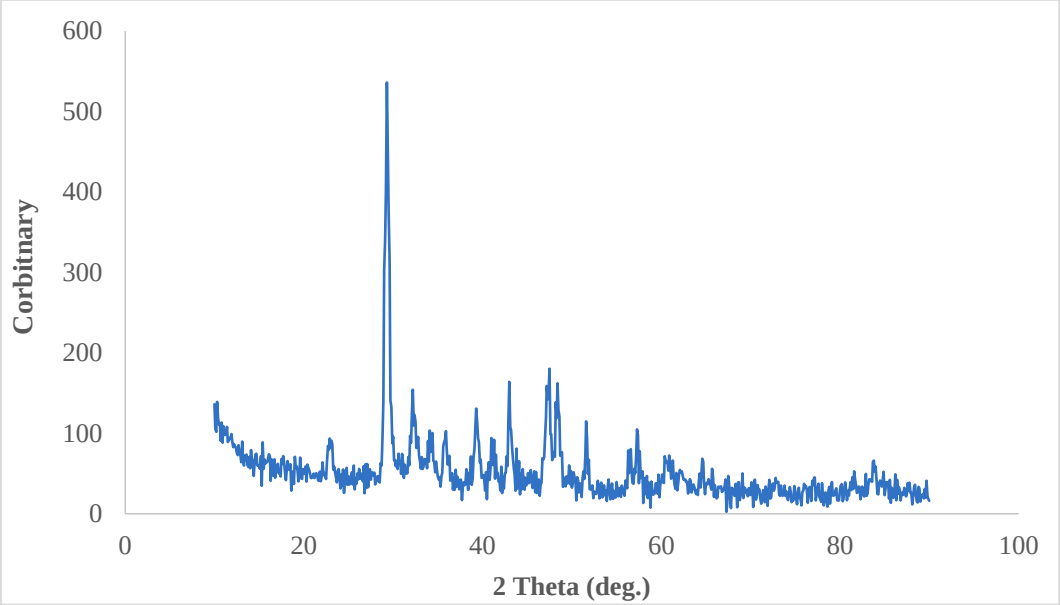

Fig. 6. XRD analysis of the 5% tincal added sample.

Tincal, dolomite, smectite, and calcite are observed in the planes corresponding to the prominent peaks in the XRD spectrum of tincal ore. The high-intensity peak observed at approximately 29° 2θ in the obtained diffractogram reveals the dominant presence of tincal ($Na_2B_4O_7.10H_2O$) and calcite ($CaCO_3$) phases in the sample. Calcite is a common component in the cement matrix, and its presence may be due to either the clinker structure or the carbonation process of the cement matrix. In addition, other intense peaks observed in the 32–34° 2θ range indicate the presence of calcium silicate hydrate (C-S-H) and ettringite phases, which are cement hydration products.

Some intense peaks detected in the graph with low intensity but distinct levels can be associated with X-ray reflections of the crystal structure of the mineral tincal ($Na_2B_4O_7{\cdot}10H_2O$), which is used as an additive. This suggests that the additive is preserved either physically or chemically within the cement matrix and integrated into the structure. However, diffraction intense peaks appearing between 40° and 50° 2θ suggest that tincal may have interacted with cement hydration products, triggering the formation of new mineral phases.

These data indicate that a 5% tincal addition can lead to the formation of specific crystalline phases in the cement matrix, thereby inducing structural changes in the cement microstructure. Such structural changes have the potential to directly affect the mechanical and physical properties (e.g., compressive strength, durability, and impermeability) of cement-based composites.

3.4. SEM analysis findings (5% tincal added sample)

The SEM image of a cement sample containing 5% Tincal additive, obtained after a 7-day curing period, provides important data about the microstructural characteristics of the material. Images a) were obtained at 1000x magnification with a 100 µm scale bar, b) at 2500x magnification with a 50 µm scale bar, c) at 5000x magnification with a 20 µm scale bar, and d) at 10000x magnification with a 10 µm scale bar. The SEM images show that the the tincal ore structure generally consists of short prismatic crystals, partly platy and flat crystals, and the grains have smooth surfaces (Fig. 7).

Table 4. Average compressive strengths of the mixtures.

Group no	Group number	Compressive strength (MPa)	Avg. comp. strength (MPa)
1	Control-1	31.54	
2	Control-2	33.14	32.4
3	Control-3	32.53	
4	Control + Tincal 5%	2.01	
5	Control + Tincal 5%	2.02	2.02
6	Control + Tincal 5%	2.03	

3.5. Unconfined compression test of tincal-added cement

After a 7-day curing period in saturated water, 3 samples were taken from each mixture and subjected to compressive strength testing. The average compressive strength values of the samples from the mixtures are given in Table 4 and Fig. 8.

The data in Table 4 allows for the comparative evaluation of the compressive strength performance of cement-based concrete samples containing 5% Tincal additive with the control group. While the average compressive strength in the control group samples was determined as 32.4 MPa, this value remained at only 2.02 MPa in the Tincal-added concrete samples prepared under the same conditions. This result shows that Tincal additive has a significantly adverse effect on mechanical strength at early ages.

This significant loss of strength suggests that Tincal interferes with the cement hydration process or negatively affects the formation of the binder matrix. Possible causes include reactive incompatibility of Tincal's chemical composition with the cement or its role in inhibiting the development of hydration products. The findings indicate that Tincal should be investigated comprehensively, not only in terms of its photon or neutron attenuating potential, but also in terms of its effects on the structural performance of concrete.

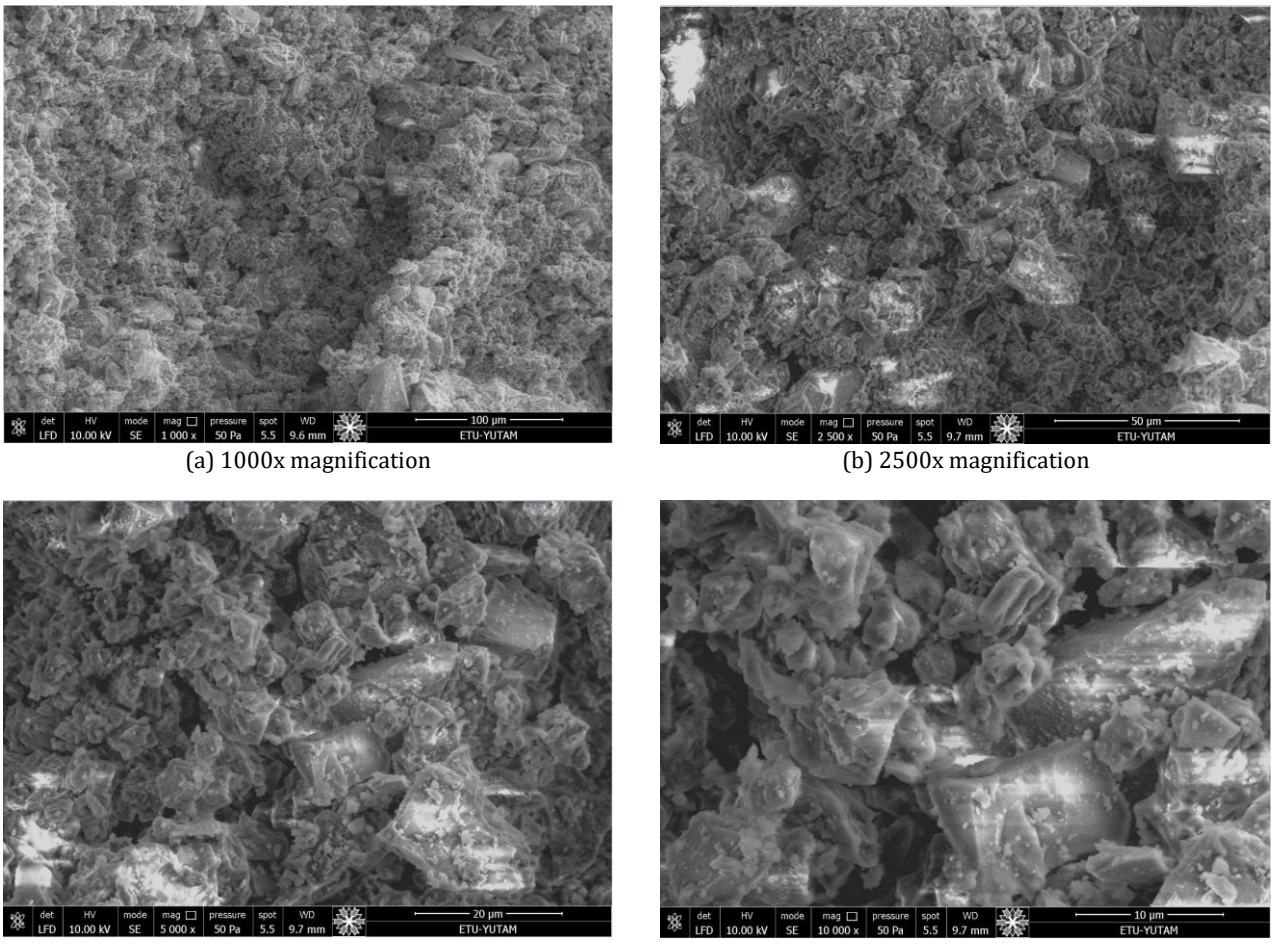

(a) 1000x magnification (b) 2500x magnification

(c) 5000x magnification (d) 10000x magnification

Fig. 7. SEM image of the tincal-doped sample at different scales.

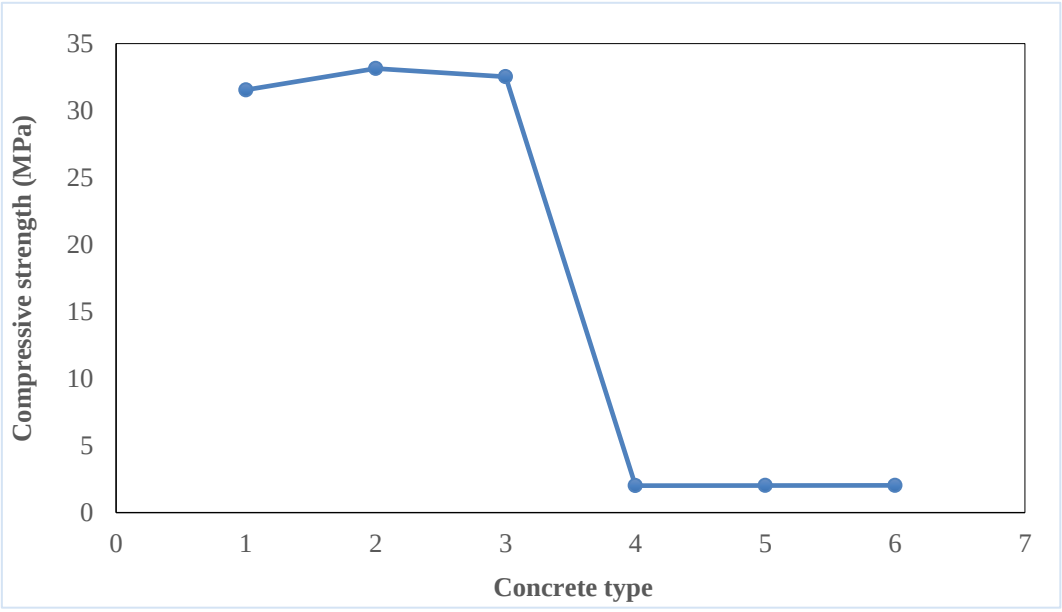

Fig. 8. Compressive strength according to mix type.

4. Conclusions

In this study, the gamma and neutron attenuation properties of tincal ores obtained from the Balıkesir-Bigadiç region were investigated using various experimental methods. The experimental studies included gamma and neutron attenuation experiments under different parameters, compressive strength tests, and scanning electron microscopy (SEM) and X-ray diffraction (XRD) analyses. The results of these analyses provided a detailed evaluation of the gamma and neutron attenuation properties of the tincal ore, and the findings are presented below.

- The mass attenuation coefficients (μ/ρ) of composite samples formed by doping tincal ore at different rates were investigated experimentally. As a result of measurements carried out at energy range of 13.375 keV and 385.851 keV, it was determined that the additives had significant effects on radiation permeability, especially in the low and medium energy ranges.
- Tincal-doped samples were found to generally have higher gamma ray transmittance, leading to lower attenuation performance. A decreasing trend in the mass attenuation coefficient of the sample was observed with increasing doping ratio, and this was particularly evident in the high-energy gamma rays.
- The neutron attenuation properties of composite samples formed by adding tincal ore at different rates were experimentally investigated. It was observed that as the tincal addition rate increased, the transmitted radiation intensity decreased, while at the same time, the attenuation properties became more effective against neutrons. This obviously attribute to high nuclear reaction cross sections between boron nuclei, especially ^{10}B isotopes, and fast neutrons. It is the result of interactions between neutrons and boron nuclei.
- Demonstrating the attenuation performance of tincal ore against neutron radiation with varying amounts of additives suggests that these natural minerals can be considered alternative shielding materials in radiation protection applications. As a result, the utilization of tincal ore obtained from the Bigadiç region, one of Türkiye's important boron reserves, allows for the transformation of domestic mineral resources into value-added products. This contributes to economic sustainability and provides a strategic contribution to reducing external dependence.
- The attenuation coefficients obtained over a wide energy range constitute an important database that can be used in the design and development of next-generation radiation shielding materials. These data are a reference for the scientific literature as they form the basis for advanced research.
- The development of attenuating composites using natural minerals minimizes the production of toxic waste, contributing to the widespread adoption of environmentally friendly material technologies. In this respect, the study can be evaluated within the scope of sustainable engineering practices.
- The neutron attenuation coefficients obtained in this study were quantitatively compared with boron-based materials commonly used in the literature. The mass neutron attenuation coefficients (0.095–0.110 cm^2/g) of cement samples containing 5% tincal additive are found to be of the same order of magnitude as the values reported for concrete containing colemanite and ulexite additives (Erdoğan et al. 1998; Erdoğmuş et al. 2011; Kharita et al. 2008).
- Boron carbide (B_4C) offers higher neutron removal coefficient due to its high boron content; however, its high cost, processing difficulties, and problems with homogeneous distribution in the cement matrix limit its use in building materials (Henrie 1962). In contrast, natural boron minerals such as tincal represent an important alternative for concrete and cement-based radiation shielding applications due to their economic, environmental, and sustainable properties.
- In this context, the neutron attenuation performance of tincal-modified cement is competitive with boron-based systems in the literature, not only in terms of absolute values but also in terms of applicability and cost-effectiveness criteria.

Consequently, unless new evidence is provided demonstrating that tincal or similar boron mineral additives can match or exceed the neutron attenuation performance of these more effective boron compounds under comparable conditions, the suitability of the tested material for structural applications remains questionable. This conclusion is of particular pertinence when considering design criteria that must balance radiation shielding efficacy with mechanical integrity and durability in load-bearing concrete structures. After evaluating all the data, it was concluded that the developed structural material would be more suitable as a surface coating material rather than for use in load-bearing elements.

Since the aim of this study was to investigate the radiation permeability of cement-boron mixtures, mechanical strength was not investigated in detail. While other studies are being conducted on that topic, this information is not included in this work.

Acknowledgements

This research has previously been presented at the 8th International Eurasian Conference on Biological and Chemical Sciences (EurasianBioChem 2025) held in Ankara, Türkiye, on December 17-19, 2025. Extended version of the research has been submitted to Challenge Journal of Concrete Research Letters and has been peer-reviewed prior to the publication.

Funding

The authors received no financial support for the research, authorship, and/or publication of this manuscript.

Conflict of Interest

The authors declare no potential conflicts of interest with respect to the research, authorship, and/or publication of this manuscript.

Data Availability

The datasets generated and/or analyzed during the current study are not publicly available but are available from the corresponding author upon reasonable request.

AI Assistance

No AI-based tools were used in the preparation of this manuscript.

Author Contributions

All authors made substantial contributions to the conception and design of the study, acquisition of data, analysis and interpretation of data; drafted or critically revised the manuscript for important intellectual content; and approved the final version to be published.

REFERENCES

Abutaha F, Çelik Aİ (2025). The engineering properties of silica fume and GGBS-based geopolymer mortars cured in elevated temperature. *Challenge Journal of Concrete Research Letters*, 16(2), 69-84.

Akkurt I, Akyildirim H, Mavi B, Kilincarslan S, Basyigit C (2010). Radiation shielding of concrete containing zeolite. *Radiation Measurements*, 45(7), 827-830.

Al-Safi S, Altharehi A, Alameri IA, Al-Jolahy A (2025). The mechanical properties of cement mortar reinforced with silica fume subjected to sulfate and chloride environment. *Challenge Journal of Structural Mechanics*, 11(1), 55-69.

Ataç E (2024). The Effect of Heating Speed on the Decomposition Temperature of Tincal Ore and Calcination. *M.Sc. thesis*, Atatürk University, Erzurum, Türkiye.

Davraz M (2010). The effects of boron compounds on the properties of cementitious composites. *Science and Engineering of Composite Materials*, 17(1), 1-18.

EN 196-3 (2016). Methods of testing cement. Part 3: Determination of setting times and soundness. European Committee for Standardization, Brussels, Belgium.

Erdoğan Y, Zeybek MS, Demirbaş A (1998). Cement mixes containing colemanite from concentrator wastes. *Cement and Concrete Research*, 28, 605-609.

Erdoğmuş E, Erdoğan Y, Gencel O, Targan S, Avcıata U (2011). Influence of colemanite admixture on Portland cement durability. *Advances in Cement Research*, 24, 155-164.

Eroğlu H (2009). Adsorption of Radioactive Thallium-201 and Gallium-67 Used in Nuclear Medicine. *Ph.D. thesis*, Atatürk University, Erzurum, Türkiye.

Filazi A, Pul M (2022). Boraks pentahidrat ikamesinin çimento harcının ses geçirme ve mekanik özelliklerine etkisi. *Uluslararası Mühendislik Araştırma ve Geliştirme Dergisi*, 14(2), 604-610. (in Turkish)

Görpe A, Cantez S (1992). Temel fizik. In: Görpe A, Cantez S, editors. *Pratik Nükleer Tıp*. İstanbul Tıp Fakültesi Vakfı, İstanbul, Türkiye, 1-42. (in Turkish)

Henrie JO (1962). Concrete for Radiation Shielding. 2nd ed. American Concrete Institute, Detroit, MI, USA.

Karakoç A (2024). Making Radiation Detector and Radiation Measurement of Various Materials. *M.Sc. thesis*, Erzincan Binali Yıldırım University, Erzincan, Türkiye.

Keskin N (2024). Evaluation of the Knowledge Levels and Attitudes of Anesthesia Technicians Working in Türkiye about Protection from Ionizing Radiation. *M.Sc. thesis*, Ufuk University, Ankara, Türkiye.

Kharita MH, Takeyeddin M, Alnassar M, Yousef S (2008). Development of special radiation shielding concretes using natural local materials and evaluation of their shielding characteristics. *Progress in Nuclear Energy*, 50, 33-36.

Kiani MA, Outokesh M, Ahmadi SJ (2025). Development of a new multifunctional polymer-based nanocomposite for neutron shielding applications. *Scientific Reports*, 15(1), 45137.

Kim YK, Lim IJ, Lim H, Joo Y, Park J, Hossain MM, Cho H, You NH, Ahn S, Lee H, Lee SS, Joo Y, Moon SY, Yoo HI, Lum C, Park C, Choi SQ (2025). High-density boron nitride nanotube composites via surfactant-stabilized lyotropic liquid crystals for enhanced space radiation shielding. *Advanced Functional Materials*, 35(52), e10716.

Kocadağistan ME, Arslan H (2024). Advantageous approach for boron ores used in cement production: Optimization of dehydration. *Challenge Journal of Concrete Research Letters*, 15(1), 7-19.

Korkut T, Karabulut A, Budak G, Aygün B, Gencel O, Hançerlioğulları A (2012). Investigation of neutron shielding properties depending on number of boron atoms for colemanite, ulexite and tincal ores by experiments and FLUKA Monte Carlo simulations. *Applied Radiation and Isotopes*, 70, 341-345.

Kratochvíl J, Opravil T, Diviš P (2014). The effect of boron and its compounds on setting of Portland cement. *Advanced Materials Research*, 1000, 16-19.

Olgun A, Kavas T, Erdogan Y, Once G (2007). Physico-chemical characteristics of chemically activated cement containing boron. *Building and Environment*, 42(6), 2384-2395.

Özdemir M, Öztürk NU (2003). Utilization of clay wastes containing boron as cement additives. *Cement and Concrete Research*, 33(10), 1659-1661.

Ramachandran VS, Beaudoin JJ (2001). Handbook of Analytical Techniques in Concrete Science and Technology. Noyes Publications, Norwich, NY, USA.

Sehhatigdiri A (2014). Experimental Investigation of the Shielding Properties of Different Clays against Radioactive Materials. *M.Sc. thesis*, Atatürk University, Erzurum, Türkiye.

Shaheen YBI, Etman ZA, Sabiha HL (2025). Design of reactive powder concrete mortar mixes through high strength and durability. *Challenge Journal of Concrete Research Letters*, 16(3), 142-154.

Singh VP, Badiger NM (2014). Gamma ray and neutron shielding properties of some alloy materials. *Annals of Nuclear Energy*, 64, 301-310.

Solé VA, Papillon E, Cotte M, Walter P, Susini J (2007). A multiplatform code for the analysis of energy-dispersive X-ray fluorescence spectra. *Spectrochimica Acta Part B: Atomic Spectroscopy*, 62, 63-68.

Srivastava A, Mishra A, Singh SK (2025). Mechanical and durability study of nano-SiO2 and nano-TiO2 on fiber reinforced concrete. *Challenge Journal of Concrete Research Letters*, 16(1), 33-39.

Sychev BS, Mal'kov VV, Komochkov MM, Zaitsev LI (1967). Penetration of heavy concrete shields by high-energy neutrons. *Journal of Nuclear Energy*, 21(3), 315-317.

Tarhan İH, Tarhan Y (2025). Nonlinear in-plane response of 3D-printed concrete walls with varied infill patterns: Experimental mix design and numerical structural assessment. *Challenge Journal of Structural Mechanics*, 11(3), 160-173.

Turan E, Alameri IA, Oltulu M (2025). Long-term durability of red mud-modified cement mortars: Effects of high temperature and freeze-thaw cycles. *Challenge Journal of Structural Mechanics*, 11(3), 116-127.

Uğurlu A, Özdemir M, Topçu İ (2004). Evaluation of boron containing clay wastes in cement. *Proceedings of the 2nd International Boron Symposium*, Eskişehir, Türkiye, 405-411.

Uzbaş B (2019). Modeling of SEM and XRD-Supported Visual Analyses of Cement-Based Composites Containing Silica Fume and Fly Ash Using Artificial Neural Networks. *Ph.D. thesis*, Atatürk University, Erzurum, Türkiye.

Wang P, Tang X, Chai H, Chen D, Qiu Y (2015). Design, fabrication, and properties of a continuous carbon-fiber reinforced Sm_2O_3/polyimide gamma ray/neutron shielding material. *Fusion Engineering and Design*, 101, 218-225.

Winter NB (2012). Scanning Electron Microscopy of Cement and Concrete. WHD Microanalysis Consultants Ltd., Woodbridge, UK.

Yang S, Yao Y, Wang H, Huang H (2024). A comparative study of neutron shielding performance in Al-based composites reinforced with various boron-containing particles for radiotherapy: A Monte Carlo simulation. *Nanomaterials*, 14(21), 1696.

Yılmaz E (2011). Determination of Gamma Ray Attenuation Coefficients and Neutron Removal Cross Sections in Some Building Materials. *M.Sc. thesis*, Rize University, Rize, Türkiye.